

Assessment of MODIS-derived visible and near-IR aerosol optical properties and their spatial variability in the presence of mineral dust

J. Redemann,¹ Q. Zhang,¹ B. Schmid,¹ P. B. Russell,² J. M. Livingston,³ H. Jonsson,⁴ and L. A. Remer⁵

Received 19 April 2006; revised 9 August 2006; accepted 24 August 2006; published 30 September 2006.

[1] Mineral dust aerosol is among the most difficult aerosol species to measure quantitatively from space. In this paper, we evaluate MODIS retrievals of spectral aerosol optical depth (AOD) from the visible to the near-IR off the US West Coast using measurements taken by the NASA Ames Airborne Tracking Sunphotometer, AATS-14, during the EVE (Extended-MODIS- λ Validation Experiment, 2004) campaign in April of 2004. In EVE, a total of 35 and 49 coincident over-ocean suborbital measurements at the nominal level-2 retrieval scale of 10 km \times 10 km were collected for Terra and Aqua, respectively. For MODIS-Terra about 80% of the AOD retrievals are within the estimated uncertainty, $\Delta\tau = \pm 0.03 \pm 0.05\tau$; this is true for both the visible (here defined to include 466–855 nm) and near-IR (here defined to include 1243–2119 nm) retrievals. For MODIS-Aqua about 45% of the AOD retrievals are within $\Delta\tau = \pm 0.03 \pm 0.05\tau$; the fraction of near-IR retrievals that fall within this uncertainty range is about 27%. We found an rms difference of 0.71 between the sunphotometer and MODIS-Aqua estimates of the visible (553–855 nm) Ångström exponent, while the MODIS-Terra visible Ångström exponents show an rms difference of only 0.29 when compared to AATS. The cause of the differences in performance between MODIS-Terra and MODIS-Aqua could be instrument calibration and needs to be explored further. The spatial variability of AOD between retrieval boxes as derived by MODIS is generally larger than that indicated by the sunphotometer data. **Citation:** Redemann, J., Q. Zhang, B. Schmid, P. B. Russell, J. M. Livingston, H. Jonsson, and L. A. Remer (2006), Assessment of MODIS-derived visible and near-IR aerosol optical properties and their spatial variability in the presence of mineral dust, *Geophys. Res. Lett.*, 33, L18814, doi:10.1029/2006GL026626.

1. Introduction

[2] Mineral dust aerosol has both a direct and indirect radiative effect on climate [e.g., Sokolik *et al.*, 2001], yet it is among the most difficult aerosol species to measure quantitatively from space. The observational challenges stem from the lack of knowledge on dust particle shape and absorption, and from the spatial inhomogeneity of dust plumes, which makes it difficult for certain cloud masking

techniques to distinguish them from cirrus clouds. Several field campaigns in recent years have been partially devoted to evaluating satellite retrievals of mineral dust properties [e.g., Reid *et al.*, 2003]. The timing and location of the EVE (Extended-MODIS- λ Validation Experiment, 2004, discussed here) campaign were specifically chosen to maximize the chance of encountering transport events of mineral dust to the US West coast.

[3] The objectives of this paper are threefold. First, we evaluate the retrievals of aerosol properties by MODIS-Aqua and MODIS-Terra during the EVE campaign. We compare quantitatively the MODIS retrievals of spectral AOD at seven wavelengths and two Ångström exponents, one visible and one near-IR, to measurements made by the 14-channel NASA Ames Airborne Tracking Sunphotometer (AATS-14) aboard the CIRPAS Twin-Otter aircraft during April 16–30, 2004. Importantly, the AATS-14 measurements were taken over the dark ocean within exactly collocated MODIS retrieval boxes, extending spectrally beyond 2119 nm, i.e. the longest wavelength for MODIS AOD retrievals. Secondly, because the sunphotometer measurements captured both Terra and Aqua overpasses, we can compare quantitatively the performance of the aerosol retrievals from the MODIS instruments on the two satellites to each other. Finally, we compare the spatial variability between the MODIS retrievals of AOD and Ångström exponents to the airborne sunphotometer measurements on scales of up to 150 km. In this manner, we assess the ability of the MODIS instruments to identify gradients in aerosol abundance or particle properties between adjacent or multiple retrieval grid boxes.

2. Description of Data Sets

2.1. MODIS Aerosol, MO/YD04_L2

[4] The MODIS over-ocean algorithm for the retrieval of aerosol optical depth aggregates the reflectances from the six channels at 553, 644, 855, 1243, 1632 and 2119 nm into nominal 10 km boxes of 20 by 20 pixels at 500 m resolution [Remer *et al.*, 2005]. The algorithm uses the difference in spatial variability between aerosols and clouds for the identification of clouds [Martins *et al.*, 2002]. This test separates aerosol from most cloud types, but may fail for large, thick clouds and for cirrus, which can be spatially homogeneous. It may also erroneously identify inhomogeneous aerosol fields as clouds.

[5] After the application of various cloud masks, a sediment mask is applied [Li *et al.*, 2003], after which the brightest 25% and darkest 25% (at 855 nm) of the remaining pixels are discarded. The reflectances in the remaining pixels are averaged and compared to a look-up table,

¹BAER Institute, Sonoma, California, USA.

²NASA Ames Research Center, Moffett Field, California, USA.

³SRI International, Menlo Park, California, USA.

⁴CIRPAS, Marina, California, USA.

⁵NASA Goddard Space Flight Center, Greenbelt, Maryland, USA.

consisting of four fine and five coarse mode aerosol types [Remer *et al.*, 2005]. All combinations of fine and coarse mode pairs that fit the measured reflectances to within 3% (or the best three combinations if no solution fits the reflectances to within 3%) are then averaged to yield the average combination of fine and coarse mode aerosol.

[6] Examples of initial validation efforts of the MODIS level 2 aerosol data product were given by Levy *et al.* [2003, 2005] and Remer *et al.* [2005]. Remer *et al.* [2005] found that one standard deviation of all MODIS-Terra AOD retrievals (when compared to AERONET AOD measurements) fall within the predicted uncertainty $\Delta\tau = \pm 0.03 \pm 0.05\tau$ over ocean and $\Delta\tau = \pm 0.05 \pm 0.15\tau$ over land. Recently, Ichoku *et al.* [2005] found no significant difference between MODIS-Terra and MODIS-Aqua in their ability to determine AOD between 466 and 855 nm.

[7] The Scientific Data Sets (SDS) within the MODIS level-2 aerosol data products we specifically consider in this paper are the spectral AOD at 466, 553, 644, 855, 1243, 1632 and 2119 nm, the visible Ångström exponent between 553 and 855 nm, and the near-IR Ångström exponent between 855 and 2119 nm. With the exception of an effort by Levy *et al.* [2005], there has been no systematic evaluation of the MODIS near-IR aerosol retrievals. Among the unique aspects of this study is the evaluation of MODIS-retrieved aerosol optical depth and Ångström exponents beyond 855 nm. In fact, our analyses extend to 2119 nm and were made possible by the addition of a temperature-controlled channel at 2139 nm to the AATS-14 instrument in July 2002 (see next section), specifically conceived for the evaluation of MODIS near-IR aerosol retrievals.

2.2. AATS-14

[8] AATS-14 measures direct solar beam transmission in narrow channels (with bandwidths between 2 and 5.6 nm for the wavelengths between 354 and 1558 nm and 17.3 nm for the 2139 nm channel) by using detectors in a tracking head that is mounted externally to the aircraft. From the measured slant-path transmissions we derive the aerosol optical depth (AOD), $\tau(\lambda)$, in 13 wavelength bands at 354, 380, 453, 499, 519, 604, 675, 778, 864, 1019, 1240, 1558 and 2139 nm and the columnar amounts of H₂O [Schmid *et al.*, 2001] and O₃. The two channels at 1558 and 2139 nm are temperature-controlled at 0°C; all other channels are controlled at 45°C. AATS-14 data are corrected for Rayleigh scattering and absorption by O₃, NO₂, H₂O and O₂-O₂. Measurements in previous deployments and methods for data reduction and error analysis have been described previously [Russell *et al.*, 1999; Livingston *et al.*, 2003].

[9] Radiometric calibration of AATS-14 is determined using the Langley plot technique [Schmid and Wehrli, 1995]. For EVE, AATS-14 was calibrated at the Mauna Loa Observatory, Hawaii, in March and June of 2004, bracketing the EVE campaign. Due to filter degradation, the calibration constants obtained from the post-mission calibration were generally lower than the pre-mission calibration. However, for eleven of the thirteen aerosol channels the change was 0.5% or less. The two remaining channels (380 and 1240 nm) had degraded by about 1%. We assumed a linear temporal variation between the pre- and post-

mission calibration constants, considering their change by including a statistical uncertainty equal to half the range between pre- and post-mission calibration. Because sunphotometers have a non-zero field of view, they measure some diffuse light in addition to the direct solar beam. As a result, uncorrected sunphotometer measurements can overestimate direct-beam transmission and hence underestimate $\tau(\lambda)$. This effect increases with decreasing wavelength and increasing particle size. We estimated these diffuse light effects using formulations derived by Russell *et al.* [2004], which are applicable over a wide range of column particle size distributions.

[10] After consideration of all possible sources of error, the AATS-14 derived AOD had the highest uncertainties for those channels with the largest difference in pre- and post-mission calibration. For example, the uncertainties in AOD at 380 nm during Aqua overpass time on March 26, 2004, at a mean aerosol air mass factor of 1.2, yielded a mean value of 0.008, while the average uncertainty in the 1240 nm AOD was 0.005.

3. Results

[11] In the period from April 16 to April 30, 2004, the CIRPAS Twin-Otter aircraft flew seven research flights, each focused on measurements off the Northern California coast outside of MODIS glint, but inside an area with satellite elevation angles greater than 30 degrees. During these flights, AATS-14 (deployed on the Twin-Otter aircraft) captured four MODIS-Terra (April 16, 21, 26 and 28) and four MODIS-Aqua (April 21, 26, 28 and 30) overpasses, collecting coincident measurements within a total of 35 and 49 10x10 km aerosol retrieval boxes for Terra and Aqua, respectively. As an example, Figure 1 shows the true color MODIS image, and retrieval maps of aerosol optical depth at 553 nm and the visible (553 to 855 nm) Ångström exponent in the study area off of Monterey Bay, for the Terra overpass (upper row) and Aqua overpass (lower row) on April 26, 2004.

3.1. Aerosol Optical Depth Comparisons

[12] All suborbital measurements considered in this paper were taken within ± 30 minutes of satellite overpass time at aircraft altitudes below 80 m (usually at altitudes of 30–40 m). Within each grid box, the AATS-14 measurements of AOD were averaged to yield a spectrum, which was then fitted with a quadratic least-square fit of $\log(\tau)$ versus $\log(\lambda)$. From the AATS-fit, the AOD at the intermediate MODIS wavelengths of 466, 553, 644, 855, 1243, 1632 and 2119 nm was determined. Although some MODIS wavelengths are represented within the AATS-14 spectrum, the fit procedure above was used to minimize the impact of possible AATS-14 single-channel contamination, calibration uncertainties and uncertainties stemming from gaseous absorption at the near-IR wavelengths.

[13] Figures 2a and 2c show scatter plots of MODIS-Terra (Figure 2a) and MODIS-Aqua (Figure 2c) versus AATS-14 derived AOD. Figures 2b and 2d show the difference between the AATS-14 and MODIS-derived spectral AOD versus AATS-derived visible Ångström exponent (553–855 μnm). It is apparent that a larger number of MODIS-Aqua than MODIS-Terra retrievals of AOD falls

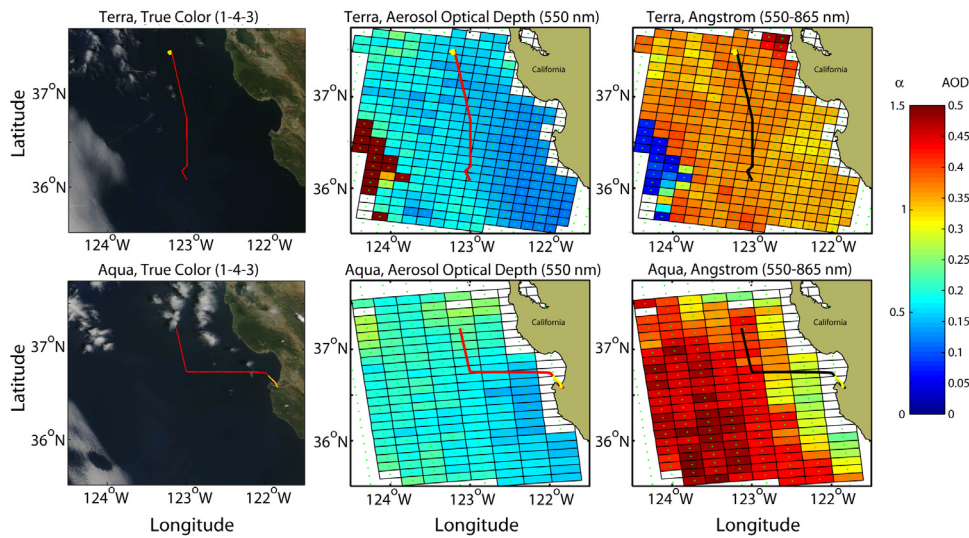


Figure 1. MODIS true color image (bands 1, 4 and 3), and the retrieval maps of aerosol optical depth at 553 nm and the visible Ångstrom exponent (553–855 nm) in the study area off Monterey Bay, for the (top row) Terra and (bottom row) Aqua on April 26, 2004. The low-altitude aircraft tracks are plotted as red or black lines.

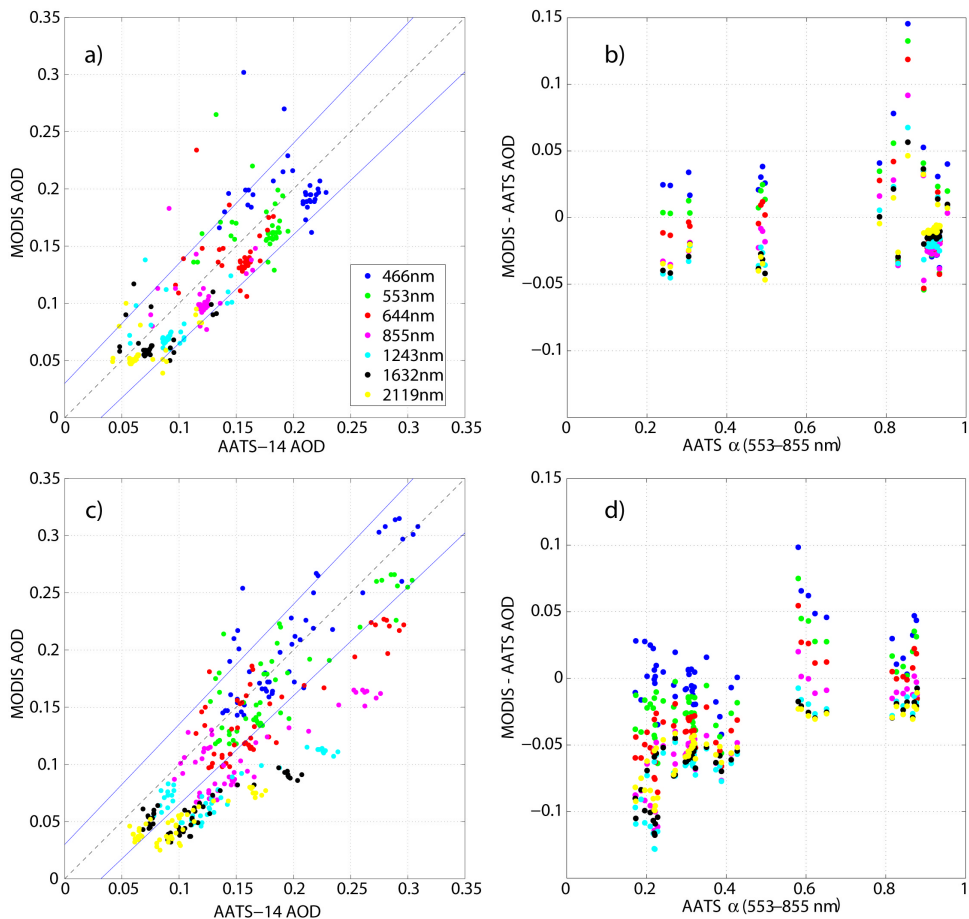


Figure 2. (a) Scatter plots of 35 retrievals of MODIS-Terra and AATS-14 derived spectral aerosol optical depth in EVE. Also shown are the MODIS uncertainty estimates of $\Delta\tau = \pm 0.03 \pm 0.05\tau$ as blue lines. (b) Difference between AATS-14 and MODIS-Terra derived spectral AOD versus AATS-derived visible Ångstrom exponent (553–855 nm). (c) Same as Figure 2a but for 49 MODIS-Aqua aerosol retrievals. (d) Same as Figure 2b, but again for 49 MODIS-Aqua aerosol retrievals.

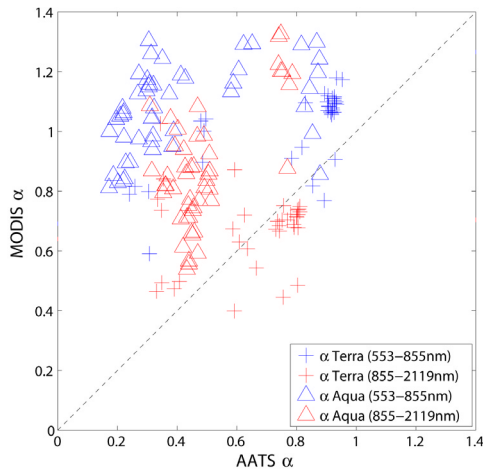


Figure 3. Scatter plot comparison of visible (553–855 nm, blue symbols) and near-IR (855–2119 nm, red symbols) Ångström exponents for MODIS-Terra (crosses) and MODIS-Aqua (triangles) versus AATS-14 derived Ångström exponents.

outside of the uncertainty estimate when compared to AATS-14, with most MODIS-Aqua retrievals underestimating the AATS-14 retrievals. For MODIS-Terra about 80% of the AOD retrievals are within the estimated uncertainty, $\Delta\tau = \pm 0.03 \pm 0.05\tau$; this is true for both the visible (466–855 nm) and near-IR (1243–2119 nm) retrievals. For MODIS-Aqua about 45% of the AOD retrievals are within $\Delta\tau = \pm 0.03 \pm 0.05\tau$; the fraction of near-IR retrievals within this uncertainty range is about 27%. Figure 2d shows that the majority of these cases occurs at Ångström exponents of 0.4 or less, i.e., those cases when the full column AOD is dominated by large particles. By comparison, the small number of MODIS-Terra AOD retrievals in the Ångström exponent range below 0.4 shows no sign of underestimating AATS-14 AOD.

3.2. Ångström Exponent Comparisons

[14] Similar to the methodology used for the AOD comparisons in the previous section, we determined visible and near-IR Ångström exponents from the AATS-14 measurements within MODIS retrieval boxes by first averaging all AATS-14 AOD measurements, then fitting them with a quadratic, and finally calculating the Ångström exponents from the ratios of the fitted AOD (τ_{fit}) at the respective wavelengths, viz.:

$$\alpha = -\frac{\ln[\tau_{fit}(\lambda_1)/\tau_{fit}(\lambda_2)]}{\ln(\lambda_1/\lambda_2)} \quad (1)$$

where the wavelength pairs are 553 and 855 nm for the visible and 855 and 2119 nm for the near-IR Ångström exponent, respectively. Figure 3 shows a scatter plot comparison of visible (blue symbols) and near-IR (red symbols) Ångström exponents for MODIS-Terra (crosses) and MODIS-Aqua (triangles). With the exception of the near-IR MODIS-Terra Ångström exponents (red crosses), there is very poor agreement between the AATS-14 and MODIS derived Ångström exponents. In general, the MODIS-derived values of Ångström exponents overestimate the AATS-derived values. This is particularly true for the smaller absolute values in Ångström exponents. The rms-differences between AATS-14 and MODIS-derived visible Ångström exponents are 0.29 (36%) for MODIS-Terra and 0.71 (173%) for MODIS-Aqua; the rms-differences between AATS-14 and MODIS-derived near-IR Ångström exponents are 0.21 (33%) for MODIS-Terra and 0.42 (85%) for MODIS-Aqua. None of the four r^2 -correlation coefficients is greater than 0.49.

3.3. Spatial Variability of Aerosol Optical Depth and Ångström Exponents

[15] In this section we evaluate the MODIS aerosol retrievals in terms of their ability to reproduce the spatial variations seen in the suborbital measurements. Specifically, Figure 4a shows a scatter plot of the change in AOD, $\Delta\tau$, at 553 nm and 2119 nm between adjacent MODIS retrieval boxes as determined by MODIS-Terra (crosses) and MODIS-Aqua (triangles), respectively, versus collocated AATS-14 measurements. (b) Same as Figure 4a, but for the change in visible (553–855 nm) and near-IR (855–2119 nm) Ångström exponents, $\Delta\alpha$, between adjacent MODIS retrieval boxes.

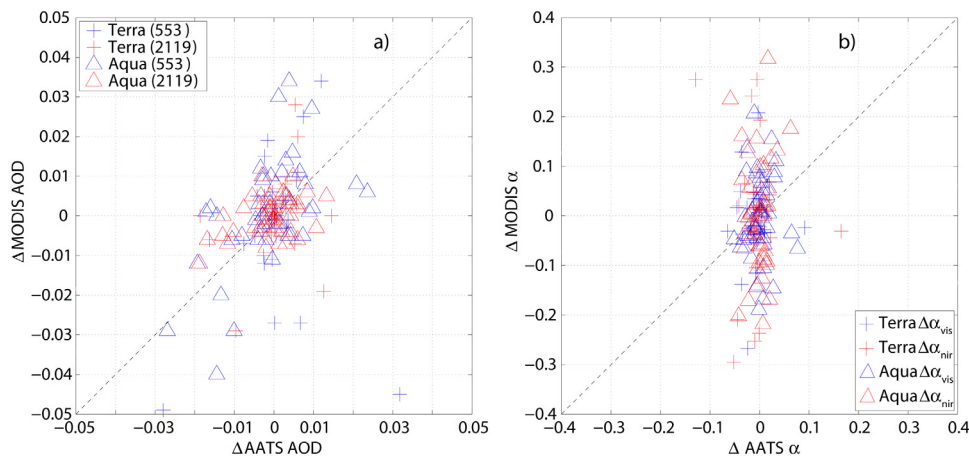


Figure 4. (a) Scatter plot of the change in AOD, $\Delta\tau$, at 553 nm and 2119 nm between adjacent MODIS retrieval boxes as determined by MODIS-Terra (crosses) and MODIS-Aqua (triangles), respectively, versus collocated AATS-14 measurements. (b) Same as Figure 4a, but for the change in visible (553–855 nm) and near-IR (855–2119 nm) Ångström exponents, $\Delta\alpha$, between adjacent MODIS retrieval boxes.

Table 1. Summary of Absolute Changes in AOD, $|\Delta\tau|$, and Ångström Exponents, $|\Delta\alpha|$, Between Adjacent MODIS Retrieval Boxes as Determined by MODIS and AATS-14, Respectively^a

Variable	MODIS-Terra	AATS-14	MODIS-Aqua	AATS-14
Mean/Mode of $ \Delta\tau$ (553 nm)	0.015/0.005	0.006/0.000	0.009/0.002	0.007/0.000
Mean/Mode of $ \Delta\tau$ (2119 nm)	0.003/0.000	0.005/0.000	0.004/0.000	0.005/0.000
Lag-1, $r(15$ km) of τ (553 nm)	0.25	0.96	0.96	0.98
Lag-1, $r(15$ km) of τ (2119 nm)	0.84	0.96	0.96	0.98
Mean/mode of $ \Delta\alpha_{vis} $	0.053/0.014	0.018/0.000	0.066/0.044	0.017/0.001
Mean/mode of $ \Delta\alpha_{nir} $	0.092/0.018	0.022/0.000	0.088/0.000	0.016/0.000
Lag-1, $r(15$ km) of $\Delta\alpha_{vis}$	0.88	0.99	0.85	0.99
Lag-1, $r(15$ km) of $\Delta\alpha_{nir}$	0.42	0.97	0.85	0.98

^aChanges are given for the midvisible AOD at 553 nm and the near-IR AOD at 2119 nm. Also shown are the lag-1 auto-correlation coefficients for the two AOD and the two Ångström exponents for both data sets. These were calculated using equation (2), for a length scale, k , of 15 km.

boxes as determined by MODIS and AATS-14, respectively. Figure 4b shows a plot of the change in visible (553–855 nm) and near-IR (855–2119 nm) Ångström exponents, $\Delta\alpha$, between adjacent MODIS retrieval boxes. We note that there is relatively poor agreement between the MODIS and AATS determined changes in AOD. The agreement is worse for the change in Ångström exponents; AATS-14 yields changes in the range of ± 0.1 while the MODIS retrievals yield changes of up to ± 0.3 .

[16] Table 1 summarizes the variability in the MODIS and AATS-14 data sets in terms of the means and modes of the absolute changes in AOD, $|\Delta\tau|$, and Ångström exponents, $|\Delta\alpha|$, between adjacent MODIS retrieval boxes. In the case of MODIS-Terra, AATS-14 derived changes in both AOD and Ångström exponents indicate the most likely change to be zero (i.e., mode is equal to zero), while MODIS-Terra indicates the most likely change in visible AOD to be 0.005. Similarly, the average changes in visible AOD and in both Ångström exponents as determined by MODIS-Terra are three to four times larger than those indicated by AATS-14. The discrepancy between MODIS-Aqua and AATS-14 derived Ångström exponents is similar to the MODIS-Terra comparisons, but there is better agreement between the means and modes of the AATS-14 and MODIS-Aqua derived changes in AOD at both 553 and 2119 nm. However, an analysis of the MODIS-derived cloud conditions revealed the presence of 4 points in the MODIS-Terra data set that had cloud fractions in excess of 85%. Eliminating these data points lowered the mean $|\Delta\tau|$ between adjacent retrievals to 0.0096 (down from 0.0148) for MODIS-Terra and 0.0038 (down from 0.0057) for the respective AATS retrievals. Hence, the mean variability in the MODIS-Terra AOD is still larger than that during the Aqua overpasses, but the ratio between MODIS-Terra and AATS is now about the same as between MODIS-Aqua and AATS, indicating similar performance of MODIS-Terra and MODIS-Aqua when comparable cloud conditions are considered. Also shown in Table 1 are the lag-1 auto-correlation coefficients for the two AOD and the two Ångström exponents for both data sets, calculated using the following formulation for the auto-correlation function, adapted from Anderson *et al.* [2003]:

$$r(k) = \frac{\sum_i^N [(x_i - m_{+k})(x_{i+k} - m_{-k})]}{(N-1)s_{+k}s_{-k}} \quad (2)$$

where k indicates the spatial lag (or distance), m_{+k} and s_{+k} denote the mean and standard deviation, respectively, of all data points that are located a distance of “+ k ” away from another data point, and m_{-k} and s_{-k} are the corresponding quantities for data points located a distance of “− k ” away from another data point. At the smallest available spacing (~ 0.2 km for the AATS-14 retrievals in EVE), the lag-1 auto-correlation assesses both the natural variability and instrumental noise. At this scale the AATS-14 lag-1 auto-correlation always measured greater than 0.99, indicating small instrumental noise and also small natural variability. Table 1 compares the auto-correlation of MODIS and AATS-14 determined AOD and Ångström exponent between adjacent MODIS retrieval boxes. We set the lag-distance to $k = 15$ km, and calculated $r(k)$ for all quantities shown in Figure 4. Table 1 shows that all AATS derived AOD and Ångström exponents yield auto-correlations of 0.96 and above. All MODIS-derived auto-correlations yield smaller values and hence suggest larger variability in the examined aerosol properties.

4. Summary

[17] Based on coincident measurements with the NASA AATS-14, we have evaluated (i) MODIS retrievals of spectral AOD from the visible to the near-IR, (ii) MODIS retrievals of the visible (553–855 nm) and near-IR (855–2119 nm) Ångström exponents, (iii) changes in AOD and Ångström exponents between adjacent MODIS retrieval boxes. The timing and location of these measurements were chosen to maximize the likelihood of encountering Asian dust transported across the Pacific Ocean, providing a measurable AOD at wavelengths beyond 855 nm. Our assessment of the presence of mineral dust is supported by NAAPS (NRL Aerosol Analysis and Prediction System) model results and by the in situ instrumentation on the aircraft (a 3- λ nephelometer, a cavity ring down spectrometer and several particle probes) which indicated the presence of large particles in layers at 4–5 km altitude in all seven research flights. However, it is possible that in a number of comparisons presented an appreciable amount of sea salt particles was present.

[18] We find that in the presence of mineral dust aerosol a larger fraction (80%) of MODIS-Terra retrievals of spectral AOD fall within the estimated over-ocean uncertainty range of $\Delta\tau = \pm 0.03 \pm 0.05\tau$ than for MODIS-Aqua (45%). In particular, only 27% of MODIS-Aqua AOD retrievals

between 1243 and 2119 nm fall within the aforementioned uncertainty range. Our analyses yield an rms difference of 0.71 between the AATS-14 and MODIS-Aqua estimates of the visible Ångström exponent, while the MODIS-Terra Ångström exponents show an rms difference of only 0.29 when compared to AATS-14. While the overestimate of visible Ångström exponents by MODIS-Terra in the presence of mineral dust has been reported previously [Levy *et al.*, 2003], the difference in performance between MODIS-Terra and MODIS-Aqua, in particular at longer wavelengths is a new finding. The cause of these differences could be instrument calibration and needs to be explored further. For example, Terra has 11 noisy and 1 inoperable detectors (out of a possible 490), while Aqua's channels are all good except the 1632 nm channel which has many dead detectors. Missing the 1632 nm channel has serious repercussions in retrieving aerosol size and spectral AOD, as most of the MODIS strength in size retrieval resides in the 1632 and 2119 nm channels.

[19] The spatial variability of AOD between retrieval boxes as derived by MODIS is larger than that indicated by the AATS-14 measurements. Larger-scale gradients in AOD are reproduced well. Spatial variability in MODIS-derived Ångström exponents between retrieval boxes is considerably larger than that measured by AATS-14 and hence appears erroneous. It should be noted that the apparent variability in the MODIS AOD retrievals is below the range of retrieval uncertainty and therefore does not affect the retrieval accuracy itself. The reason for the larger variability in the MODIS-derived AOD and Ångström exponents could be sub-pixel cloud contamination or cloud adjacency effects, which are very likely not an issue for the very conservative, fine spatial-resolution cloud screening of the AATS data set. This finding would be in accord with results reported by Kaufman *et al.* [2005], who found a correlation in differences between MODIS and suborbital AOD measurements with MODIS-derived cloud fraction. A more careful assessment of this effect on the basis of airborne sunphotometer data in multiple field campaigns in the vicinity of clouds is forthcoming, but beyond the scope of this paper.

[20] **Acknowledgments.** We gratefully acknowledge funding for this work from a grant through the NASA New Investigator Program (NIP/NAG5-12573, Program manager: M. Y. Wei) and support through an EOS grant (EOS/03-0584-0647, Program manager: H. Maring).

References

Anderson, T. L., R. J. Charlson, D. M. Winker, J. A. Ogren, and K. Holmen (2003), Mesoscale variations of tropospheric aerosols, *J. Atmos. Sci.*, *60*, 119–136.

Ichoku, C., L. A. Remer, and T. F. Eck (2005), Quantitative evaluation and intercomparison of morning and afternoon MODIS aerosol measurements

from Terra and Aqua, *J. Geophys. Res.*, *110*, D10S03, doi:10.1029/2004JD004987.

Kaufman, Y. J., et al. (2005), A critical examination of the residual cloud contamination and diurnal sampling effects on MODIS estimates of aerosol over ocean, *IEEE Trans. Geosci. Remote Sens.*, *43*, 2886–2897.

Levy, R. C., L. A. Remer, D. Tanré, Y. J. Kaufman, C. Ichoku, B. N. Holben, J. M. Livingston, P. B. Russell, and H. Maring (2003), Evaluation of the Moderate-Resolution Imaging Spectroradiometer (MODIS) retrievals of dust aerosol over the ocean during PRIDE, *J. Geophys. Res.*, *108*(D19), 8594, doi:10.1029/2002JD002460.

Levy, R. C., L. A. Remer, J. V. Martins, Y. J. Kaufman, A. Plana-Fattori, J. Redemann, P. B. Russell, and B. Wenny (2005), Evaluation of the MODIS aerosol retrievals over ocean and land during CLAMS, *J. Atmos. Sci.*, *62*, 974–992.

Li, R.-R., Y. J. Kaufman, B.-C. Gao, and C. O. Davis (2003), Remote sensing of suspended sediments and shallow coastal waters, *IEEE Trans. Geosci. Remote Sens.*, *41*, 559–566.

Livingston, J. M., et al. (2003), Airborne Sun photometer measurements of aerosol optical depth and columnar water vapor during the Puerto Rico Dust Experiment and comparison with land, aircraft, and satellite measurements, *J. Geophys. Res.*, *108*(D19), 8588, doi:10.1029/2002JD002520.

Martins, J. V., D. Tanré, L. Remer, Y. Kaufman, S. Mattoo, and R. Levy (2002), MODIS cloud screening for remote sensing of aerosols over oceans using spatial variability, *Geophys. Res. Lett.*, *29*(12), 8009, doi:10.1029/2001GL013252.

Reid, J. S., et al. (2003), Analysis of measurements of Saharan dust by airborne and ground-based remote sensing methods during the Puerto Rico Dust Experiment (PRIDE), *J. Geophys. Res.*, *108*(D19), 8586, doi:10.1029/2002JD002493.

Remer, L. A., et al. (2005), The MODIS aerosol algorithm, products and validation, *J. Atmos. Sci.*, *62*, 947–973.

Russell, P. B., J. M. Livingston, P. Hignett, S. Kinne, J. Wong, and P. V. Hobbs (1999), Aerosol-induced radiative flux changes off the United States Mid-Atlantic coast, Comparison of values calculated from sun-photometer and in situ data with those measured by airborne pyranometer, *J. Geophys. Res.*, *104*, 2289–2307.

Russell, P. B., J. M. Livingston, O. Dubovik, S. A. Ramirez, J. Wang, J. Redemann, B. Schmid, M. Box, and B. N. Holben (2004), Sunlight transmission through desert dust and marine aerosols: Diffuse light corrections to Sun photometry and pyrrometry, *J. Geophys. Res.*, *109*, D08207, doi:10.1029/2003JD004292.

Schmid, B., and C. Wehrli (1995), Comparison of sun photometer calibration by Langley technique and standard lamp, *Appl. Opt.*, *34*, 4500–4512.

Schmid, B., et al. (2001), Comparison of columnar water-vapor measurements from solar transmittance methods, *Appl. Opt.*, *40*, 1886–1896.

Sokolik, I. N., D. M. Winker, G. Bergametti, D. A. Gillette, G. Carmichael, Y. J. Kaufman, L. Gomes, L. Schuetz, and J. E. Penner (2001), Introduction to special section: Outstanding problems in quantifying the radiative impacts of mineral dust, *J. Geophys. Res.*, *106*, 18,015–18,028.

H. Jonsson, CIRPAS, 3200 Imjin Rd., Hangar 507, Marina, CA 93933, USA. (hjonsson@nps.edu)

J. M. Livingston, SRI International, G-274, 333 Ravenswood Ave., Menlo Park, CA 94025, USA. (jlivingston@mail.arc.nasa.gov)

J. Redemann, B. Schmid, and Q. Zhang, Bay Area Environmental Research Institute, 560 Third Street W, Sonoma, CA 95476, USA. (jredemann@mail.arc.nasa.gov; bschmid@mail.arc.nasa.gov; zhang@baeri.org)

L. A. Remer, NASA Goddard Space Flight Center, Code 613.2, Building 33, Room A313, Greenbelt, MD 20770, USA. (lorraine.a.remer@nasa.gov)

P. B. Russell, MS 245-5, NASA Ames Research Center, Moffett Field, CA 94035-1000, USA. (philip.b.russell@nasa.gov)